ILASS Americas 28th Annual Conference on Liquid Atomization and Spray Systems, Dearborn, MI, May 2016

A finite volume method for simulating droplet breakup in a supersonic cross flow

Daniel P. Garrick[a], Mark Owkes[b], Jonathan D. Regele[a*]

[a]Department of Aerospace Engineering
Iowa State University
Ames, IA

[b]Department of Mechanical and Industrial Engineering
Montana State University
Bozeman, MT

Abstract

Shock waves are often used in experiments to create a shear flow across liquid droplets to study secondary atomization. Similar behavior occurs inside of supersonic combustors under startup conditions, but it is not as easy to study these conditions experimentally. In order to investigate this phenomenon further, a numerical approach is developed to simulate compressible multiphase flows under the effects of surface tension forces. The flow field is solved via the compressible multicomponent Euler equations discretized with the finite volume method on a uniform Cartesian grid. The solver utilizes a total variation diminishing (TVD) third-order Runge-Kutta method for time-marching and second order limited spatial reconstruction. The Harten-Lax-van Leer contact (HLLC) approximate Riemann solver is used to upwind the fluxes. The fluid interface is captured through an additional transport equation for the volume fraction. Smearing of the fluid interface via numerical diffusion is countered using an interface compression technique applied at the end of each physical timestep. The stiffened gas equation of state is used to close the system. Surface tension is incorporated using the Continuum Surface Force (CSF) model and the required interface curvature is computed using a smoothed interface function and central differences. The multicomponent flow solver is first validated using various one and two dimensional benchmark problems before the surface tension model is verified with comparisons to the analytical values of the pressure jump specified by the Young-Laplace equation and the oscillation period of an ellipse. Finally, a preliminary investigation is performed on the effects of surface tension in a dual droplet interaction with a Mach 6 shock in air and shows the tendency of capillary forces to resist droplet deformation.

*Corresponding Author

Introduction

The current research is motivated by the importance of fuel atomization in high-speed propulsion systems. Efficient combustion is greatly dictated by the fuel-injection scheme but there is a limited understanding of the effect of design parameters on the atomization process[1], consisting of primary and secondary atomization. Primary atomization is represented by the initial breakup of a liquid sheet or jet into smaller drops or filaments. Droplets formed during primary atomization can further deform and breakup in a process known as secondary atomization. Most atomization models give the droplet size distribution in terms of the dimensionless Reynolds, Weber, or Ohnesorge numbers via empirical relationships derived from experimental measurements[1]. These dimensionless numbers are important because they relate the viscous and surface tension forces to the inertial ones. In terms of atomization, the deformation due to the aerodynamic forces is resisted by the viscous and surface tension forces[2]. Greater understanding of the physical processes in the atomization process is thus an important goal.

The multi-phase nature of the flow requires an adequate description of the interface between the gas and liquid. As most applications of primary atomization occur at low Mach numbers[3], numerical modeling has largely focused on the incompressible regime where interface tracking methods[4, 5, 6] have proven popular. Many different interface tracking methods exist and generally involve a deforming mesh, particle tracking, or an advected color function for the purposes of reconstructing the interface. Such methods guarantee a sharp interface which allows for natural modeling of immiscible fluids and interfacial physics. While many of these methods have been extended to compressible formulations[7, 8, 9, 10] they are generally geometrically complex and can be difficult to implement in multiple spatial dimensions.

The present research instead utilizes an interface capturing method[11, 12, 13]. The method is in the spirit of the shock capturing schemes already included in compressible flow algorithms and can easily handle large topology changes in the interface. The method adds an additional conservation equation to capture the fluid interface and is simple to implement in multiple dimensions. However, the method results in numerical smearing of the material interface, which in the presence of large density ratios and strong shocks can generate significant errors in computations of shock-interface interactions[14]. One option to counter numerical diffusion of the interface is implementation of high resolution WENO reconstruction[15, 16]. While the method can accurately capture material interfaces and has been successfully used to simulate the early stages of droplet breakup[17], the non-TVD nature of the WENO reconstruction may cause difficulties in computation of interface curvature, a required parameter for incorporating surface tension. Instead, the present work employs TVD spatial reconstruction with flux limiting and an interface compression technique shown to be successful in countering the numerical smearing of the interface. The method was shown to accurately compute shock-interface interaction in the presence of high density ratios and strong shocks despite being discretely non-conservative[18].

The secondary atomization process has been studied in some detail both experimentally and numerically (see [2] for a thorough review) and is characterized primarily by the Weber number which relates the surface tension and inertial forces. Surface tension has been studied in a wide variety of incompressible applications[19, 20, 21] since the development of the Continuum Surface Force (CSF) method[22] which incorporates surface tension into the fluid governing equations as a volume force. Only relatively recently has surface tension been incorporated into a compressible framework[23, 24, 25, 14, 26] where it remains a challenging problem, however as of yet, little work has been performed on the effects of surface tension on the atomization process in a supersonic crossflow and is thus the ultimate goal of the present work. Numerical simulations of atomization in this flow regime thus far have focused on the early stages of droplet breakup where surface tension effects are not expected to play a significant role[27, 17].

Details on a finite volume method developed to study the effects of secondary atomization in a supersonic crossflow is outlined in the sections that follow. Viscous effects are currently neglected in the model to provide a thorough examination of the proposed implementation of surface tension terms in isolation. This also presents a more challenging problem numerically as physical diffusion is known to counter the generation of so-called "parasitic currents" which can distort the material interface and potentially cause computational failure[28]. The overall physical model is introduced first followed by some verification simulations in one and two dimensions using previously studied model problems. Then, the curvature and surface tension terms are validated before the overall model is applied to simulation of two liquid droplets at a low Weber number in a supersonic crossflow.

Physical modeling

The five equation model of Allaire[13] is employed in conjunction with capillary force terms which feature in a non-conservative form. As such, the compressible multicomponent Euler equations govern the flowfield. The fluid components are considered immiscible and a volume fraction function is used to model the fluid interface. Mass is discretely conserved for each phase via individual mass conservation equations.

The equations are non-dimensionalized utilizing a reference density ρ_g, acoustic velocity a_0, and the droplet diameter d_0. Total energy and pressure are non-dimensionalized using $\rho_g a_0^2$. As a result of this non-dimensionalization, the surface tension terms are scaled by an acoustic Weber number. The physical Weber number is defined for a droplet with diameter d_0 in a freestream velocity u_g as

$$We = \frac{\rho_g u_g^2 d_0}{\sigma} \tag{1}$$

where ρ_g is the density of the gas and σ is the surface tension coefficient. With the Mach number defined as

$$M = \frac{u_g}{a_0} \tag{2}$$

the acoustic Weber number is determined by

$$We_a = \frac{We}{M^2}. \tag{3}$$

Surface tension is implemented as a volume force as in the CSF model[22] with terms in both the momentum and energy equations[23]. The resulting non-dimensional five equation model including capillary force terms is as follows:

$$\frac{\partial \rho_l \phi_l}{\partial t} + \nabla \cdot (\rho_l \phi_l \vec{V}) = 0, \tag{4}$$

$$\frac{\partial \rho_g \phi_g}{\partial t} + \nabla \cdot (\rho_g \phi_g \vec{V}) = 0, \tag{5}$$

$$\frac{\partial \rho \vec{V}}{\partial t} + \nabla \cdot (\rho \vec{V}\vec{V} + p\tilde{I}) = \frac{1}{We_a}\kappa \nabla \phi_l, \tag{6}$$

$$\frac{\partial E}{\partial t} + \nabla \cdot \left((E+p)\vec{V}\right) = \frac{1}{We_a}\kappa \nabla \phi_l \cdot \vec{V}, \tag{7}$$

$$\frac{\partial \phi_l}{\partial t} + \vec{V} \cdot \nabla \phi_l = 0, \tag{8}$$

where total energy is

$$E = \rho e + \frac{1}{2}\rho \vec{V} \cdot \vec{V}. \tag{9}$$

The employed non-conservative form is beneficial in that it allows for flexible treatment of the curvature term κ.

Mixture rules

The gas (g) and liquid (l) volume fractions are related by

$$\phi_g = 1 - \phi_l. \tag{10}$$

The total density is given by

$$\rho = \rho_l \phi_l + \rho_g \phi_g \tag{11}$$

with internal energy

$$\rho e = \rho_l \phi_l e_l + \rho_g \phi_g e_g. \tag{12}$$

Utilizing an isobaric assumption[13, 16] and the stiffened gas equation of state

$$p = (\gamma - 1)\rho e - \gamma \pi_\infty \tag{13}$$

the EOS parameters are given by

$$\Gamma = \frac{1}{\gamma - 1} = \frac{\phi_g}{\gamma_g - 1} + \frac{\phi_l}{\gamma_l - 1}, \tag{14}$$

$$\Pi = \frac{\gamma \pi_\infty}{\gamma - 1} = \frac{\phi_g \gamma_g \pi_{\infty,g}}{\gamma_g - 1} + \frac{\phi_l \gamma_l \pi_{\infty,l}}{\gamma_l - 1}. \tag{15}$$

The isobaric assumption has been successfully used in the past for simulating surface tension in a compressible multicomponent framework[23, 14]. Finally, the mixture speed of sound is given by

$$c = \sqrt{\frac{\gamma(p + \pi_\infty)}{\rho}} \tag{16}$$

where the mixture quantities γ and π_∞ are computed using Eqs. 14 and 15.

Interface compression

A density and interface compression technique is employed to counter the numerical diffusion of material interfaces[18]. The method provides accurate representation of the sharp interface between materials by restricting the material interface to only a few grid cells throughout the simulation. With the method, a compression step in pseudo-time τ is performed after each physical timestep:

$$\phi_\tau = \hat{n} \cdot [\nabla(\epsilon_h |\nabla \phi_l|) - \phi_l(1 - \phi_l)] \tag{17}$$

$$(\rho_l \phi_l)_\tau = H\hat{n} \cdot [\nabla(\epsilon_h \hat{n} \cdot \nabla(\rho_l \phi_l)) - (1 - 2\phi_l)\nabla(\rho_l \phi_l)] \tag{18}$$

where H restricts the density compression to the interface region using

$$H = \tanh\left[\left(\frac{\phi_l(1 - \phi_l)}{10^{-2}}\right)^2\right] \tag{19}$$

and the dissipation factor is $\epsilon_h = \frac{h}{\sqrt{2}}$ where h is the grid spacing. See[18] for more details.

Curvature

Surface tension curvature is calculated via the interface normals

$$\kappa = -\nabla \cdot \hat{n} = -\nabla \cdot \left(\frac{\nabla \psi}{|\nabla \psi|} \right) \tag{20}$$

where ψ is a smoothed interface function[18]

$$\psi = \frac{\phi_l^\alpha}{\phi_l^\alpha + (1-\phi_l)^\alpha} \tag{21}$$

with $\alpha = 0.1$ in the current simulations. The quality of the curvature calculation across the interface is then locally improved using a filtering strategy.

Discretization

The governing equations are discretized using the finite volume method on a uniform two-dimensional Cartesian grid. The resulting semi-discrete form of the equations is given by:

$$\begin{aligned} \frac{d\vec{Q}_{i,j}}{dt} =& - \left(\frac{\vec{F}_{i+1/2} - \vec{F}_{i-1/2}}{h} \right) \\ & - \left(\frac{\vec{G}_{j+1/2} - \vec{G}_{j-1/2}}{h} \right) + \vec{S}_{i,j} \qquad (22) \\ =& R(\vec{Q}_{i,j}) \qquad (23) \end{aligned}$$

where $\vec{Q}$ is the vector of state variables, $\vec{F}$ and $\vec{G}$ are the conservative convective fluxes in the x and y directions, $\vec{S}_{i,j}$ is the source term, and $R(\vec{Q}_{i,j})$ is the residual function. The fluxes are upwinded using the HLLC approximate Riemann solver[29]. To ensure oscillation free advection of material interfaces, the primitive variables are reconstructed and the HLLC features adaptions for a quasi-conservative form of the volume fraction transport equation[15]. Spatial reconstruction is performed using a TVD second order accurate scheme with the minmod limiter. The state variables are then integrated in time using the following third order TVD Runge-Kutta scheme[30]:

$$\begin{aligned} Q_{i,j}^{(1)} &= Q_{i,j}^n + \Delta t R(Q_{i,j}^n), \\ Q_{i,j}^{(2)} &= \frac{3}{4} Q_{i,j}^n + \frac{1}{4} Q_{i,j}^{(1)} + \frac{1}{4} \Delta t R(Q_{i,j}^{(1)}), \\ Q_{i,j}^{n+1} &= \frac{1}{3} Q_{i,j}^n + \frac{2}{3} Q_{i,j}^{(2)} + \frac{2}{3} \Delta t R(Q_{i,j}^{(2)}). \end{aligned} \tag{24}$$

Results and discussion

To verify the numerical model and implementation, one dimensional testing is performed first. Isolated advection of a material interface was simulated and successfully demonstrated the capability of the method to capture the interface without the onset of spurious oscillations. This was followed by a gas-liquid shock tube problem to further demonstrate the capability of the numerical method and implementation. Testing follows with interaction of a shock in air with two water columns without the effect of surface tension. Verification of the capillary force model is performed with a parasitic currents study and an oscillating ellipse test. Finally, the shock-dual droplet interaction problem is revisited with the effects of surface tension included.

Gas-liquid Riemann problem

The standard problem of isolated advection of a material interface was successfully simulated to verify the numerical scheme does not generate spurious oscillations at the material interface, however, for brevity the results are not shown here. This was followed with a gas-liquid Riemann problem previously used as a model for underwater explosions[31, 11] and verification of a multicomponent flow model[15, 16]. The problem includes highly compressed air and water at atmospheric pressure. The non-dimensional initial conditions are given by[31]:

$$(\rho_l \phi_l, \rho_g \phi_g, u, p) = \begin{cases} (0, 1.241, 0, 2.753) & -1 < x < 0 \\ (0.991, 0, 0, 3.059e-4) & 0 \le x \le 1 \end{cases} \tag{25}$$

with fluid properties $\gamma_g = 1.4, \pi_{\infty,g} = 0, \gamma_l = 5.5, \pi_{\infty,l} = 1.505$. Note the material interface is initialized with an exponential function:

$$\phi_l = \frac{1}{1 + \exp(\frac{x}{\epsilon_h})} \tag{26}$$

The results at a simulation time of $t = 0.2$ using 500 grid points, a constant timestep of $\Delta t = 1e-3$, and a single compression step per physical timestep with a compression CFL of 0.05 are shown in Fig. 1 and compare well to the exact solution.

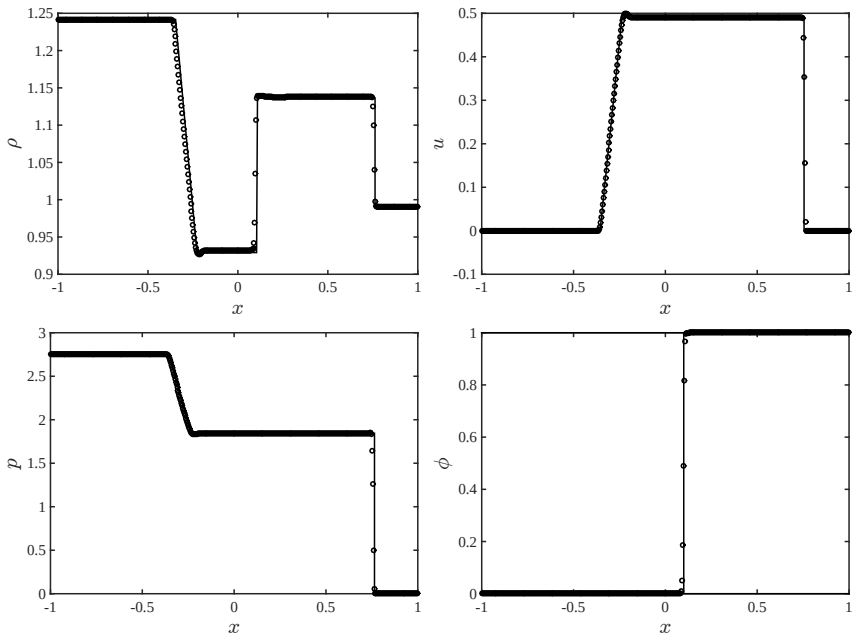

Figure 1. Final data at $t = 0.2$ using 500 grid points. Exact solution depicted by the solid line.

Dual droplet shock interaction

A Mach 6 shock in air interacting with two water columns of diameters 6.4mm and 5mm is simulated. A similar problem has been considered previously by several researchers[32, 33, 14] and is implemented here in non-dimensional form. The non-dimensionalization is given by the smaller droplet diameter $d_0 = 5mm$, the velocity $a_0 = 1000m/s$, and density by $1kg/m^3$. The domain is $[-2, 4] \times [-3, 2]$ and extrapolation boundary conditions are applied on all four boundaries. The initial conditions are given by

$$(\rho_l\phi_l, \rho_g\phi_g, u, v, p) = \begin{cases} (0, 5.268, 1.819, 0, 4.183) & x \leq -1.6 \\ (1000\phi_l, (1-\phi_l), 0, 0, 0.1) & x > -1.6 \end{cases} \tag{27}$$

where the liquid volume fraction is defined by

$$\phi_l = \frac{1}{1 + \exp(\frac{-r_1}{\epsilon_h})} + \frac{1}{1 + \exp(\frac{-r_2}{\epsilon_h})} \tag{28}$$

where $\epsilon_h = h/\sqrt{2}$, $r_1 = 0.64 - \sqrt{x^2 + y^2}$, and $r_2 = 0.5 - \sqrt{(x - 1.4)^2 + (y + 0.8)^2}$. The non-dimensional EOS parameters are $\gamma_g = 1.4, \pi_g = 0, \gamma_l = 4.4, \pi_l = 600$. Numerical schlieren (exponentially spaced normalized density gradient) results at various times are shown in Fig. 2 and agree well with the previous studies, including the ripple structures on the leading bow shock (see [32, 33, 14], for example). The transmitted and reflected shockwaves are clearly evident on the larger droplet at $t = 0.6$. The presence of the second smaller droplet results in a second reflected bow shock that interacts with and ultimately deforms the lower right quadrant of the large droplet at later times. Of particular interest will be the degree to which surface tension forces can counter this shock-interaction based deformation and the overall deformation of both droplets caused by the aerodynamic forces.

Parasitic currents

It has been suggested that improper curvature calculations can contribute to the magnitude of unphysical "parasitic currents" inherent in surface tension simulations using the CSF method[23]. Generally, these currents have been shown to scale with the inverse of the capillary number, $1/Ca = Re/We$[28, 34]. As the current work does not include physical diffusion (i.e. $Re \to \infty$, but numerical diffusion exists in practice), the effect of the parasitic currents are expected to be at their largest.

A simple test is performed to check if the currents distort the material interface. A circular liquid droplet with radius of unity is initialized in a domain $[-2, 2] \times [2, 2]$ with a zero velocity, gas density $\rho_g = 1$, liquid density $\rho_l = 1000$, pressure of unity, and extrapolation conditions applied to all four boundaries. Fluid properties are taken as in the oscillating ellipse simulation from [14] with $\gamma_g = 1.4, \gamma_l = 4.4, \pi_{\infty,g} = 0, \pi_{\infty,l} = 100$.

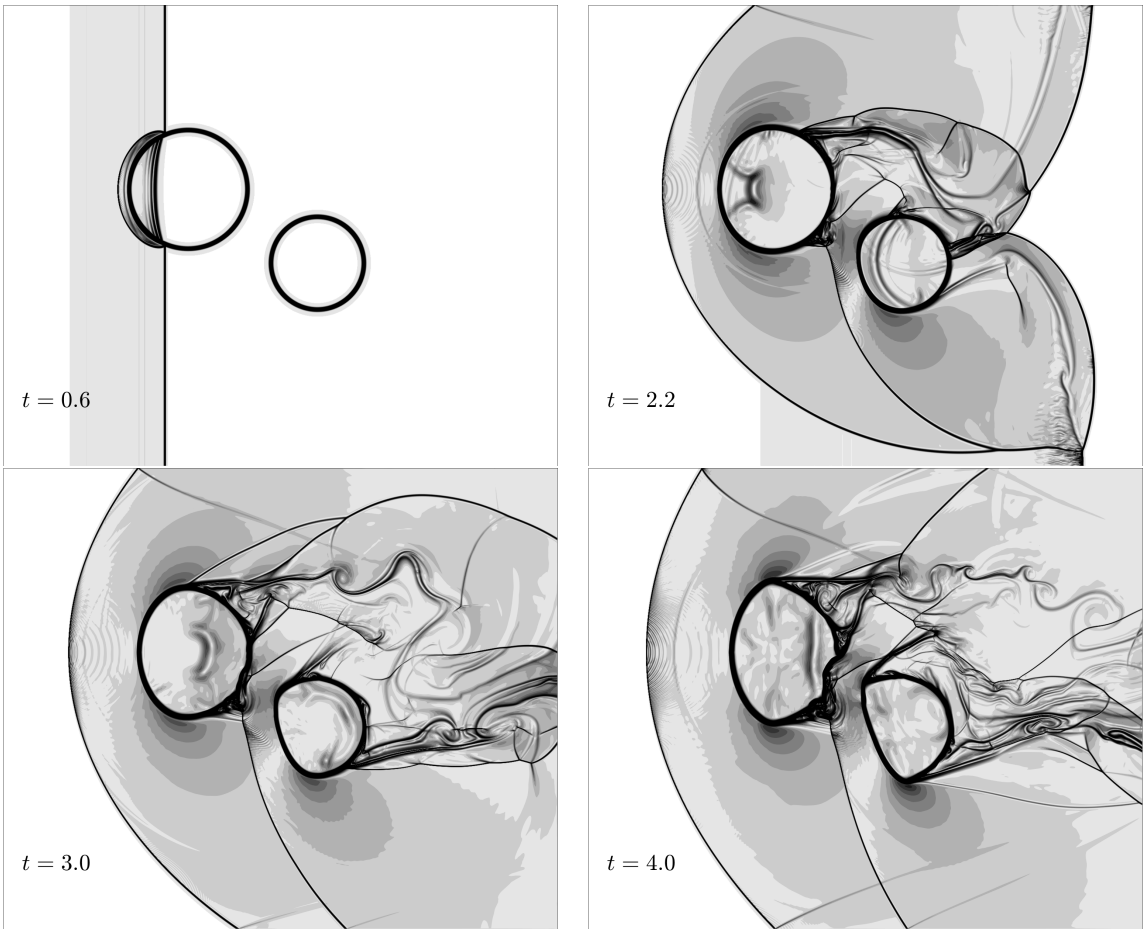

Figure 2. Dual water column shock interaction problem. Numerical Schlieren results shown in non-dimensional time. For comparison with [14], non-dimensional times shown correspond to physical times of $t = 3, 11, 15$, and $20\mu s$. Domain was discretized with a 1500×1250 grid.

The analytical pressure jump is given by the Young-Laplace law, or $\Delta p = \kappa / We_a = 1$ in this case with the acoustic Weber number set to unity. The computed pressure jump using the numerically calculated curvature values is shown in Figure 3 for a time of $t = 500$ on an 80×80 grid and agrees well with the analytical value. Additional cases were also run with a 160×160 and 320×320 grid. The maximum magnitude of the parasitic currents grew from $1.6e-3$ for the coarsest grid to $3.5e-3$ in the finest grid but never resulted in computational failure or distortion of the interface. As physical diffusion will ultimately be added to the model and should reduce the effect of parasitic currents, this is a satisfactory result.

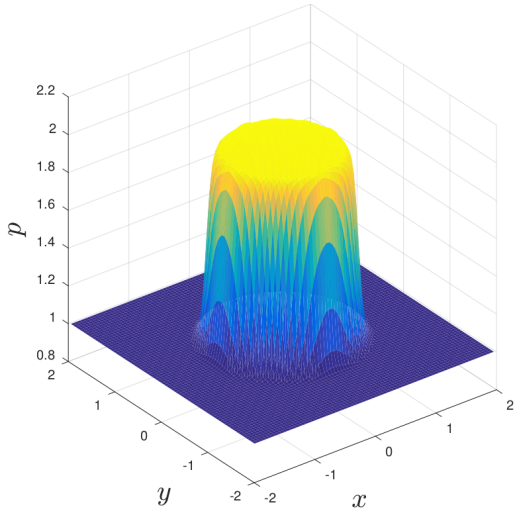

Figure 3. Computed pressure jump using numerically calculated curvature for an 80×80 grid.

Oscillating ellipse

An oscillating ellipse study is frequently performed to validate the accuracy of surface tension implementations[23, 35, 36, 14] and ensure the model is capable of predicting physical solutions. The period of oscillation can be computed analytically[37, 38]. The result has been non-dimensionalized here and is written as:

$$T = 2\pi\sqrt{\frac{We_a(1+\epsilon)R^3}{6}} \tag{29}$$

where T is the oscillation period in non-dimensional time, We_a is the acoustic Weber number, $\epsilon = \rho_l/\rho_g$ is the density ratio and R is the equivalent circular radius. An ellipse defined by

$$1 = \frac{x^2}{a^2} + \frac{y^2}{b^2} \tag{30}$$

has an equivalent circular radius of $R = \sqrt{ab}$ assuming mass is conserved. Several oscillating ellipse simulations using $a = 5/4$ and $b = 4/5$ were performed for comparison for density ratios of 100 and 1000. The domain, initial conditions, and material properties are the same as in the parasitic currents test above. The numerical oscillation period was measured using the variation in global kinetic energy and excellent agreement was found with the analytical result, as shown in Figure 4.

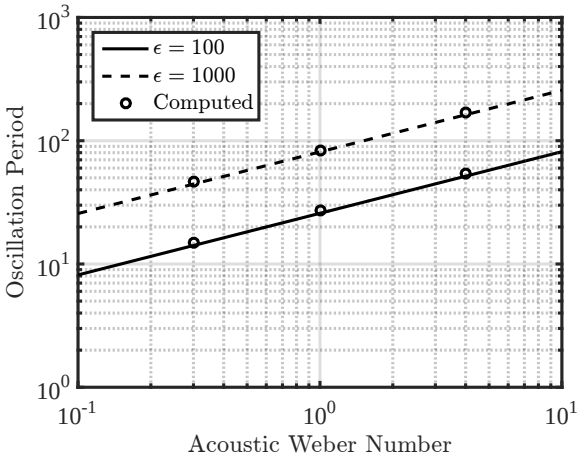

Figure 4. Analytical (lines) and computed (circles) ellipse oscillation period vs. acoustic Weber number for various density ratios ϵ.

Dual droplet shock interaction with surface tension

The compressible flow model with capillary force terms is now applied to the previously tested dual droplet shock interaction problem. Note for this problem the post-shock Mach number is 1.72 in the shock-moving reference frame and thus qualifies as a supersonic crossflow. A simulation was performed with a specified acoustic Weber number of 3.02, corresponding to a physical Weber number of 12.8 and 10 for the large and small droplets, respectively. Figure 5 shows the evolution of the interface for the simulation with and without surface tension. Droplets under the effect of surface tension tend to resist deformation due to aerodynamic forces, and that is clearly visible in the results here. This is especially evident in the lower right quadrant of the larger droplet which without surface tension undergoes significant local deformation due to the interaction of the bow shock reflected from the secondary droplet. The overall deformation has not been significantly affected by the surface tension at this timescale and significantly longer simulation times are necessary to simulate the full droplet deformation and breakup process. However, as the droplets are accelerating this requires an even larger domain size to capture and will be considered at a later time.

Conclusion

A finite volume method has been developed for simulating compressible multicomponent flow under the effects of capillary forces. The capillary terms in the compressible multicomponent flow model were validated using numerical comparisons to the analytical relationship of the oscillation period of an ellipse with various density ratios and Weber numbers. The parasitic currents did not adversely affect the interface despite physical diffusion terms being neglected at this time. The method was successfully applied to a droplet shock interaction problem in a supersonic crossflow and highlighted the effect of surface tension in combating drop deformation. Future work includes examination of droplet deformation under longer timescales and with the effects of physical diffusion.

Acknowledgments

This work is supported by Taitech, Inc. under sub-contract TS15-16-02-004 (primary contract FA8650-14-D-2316).

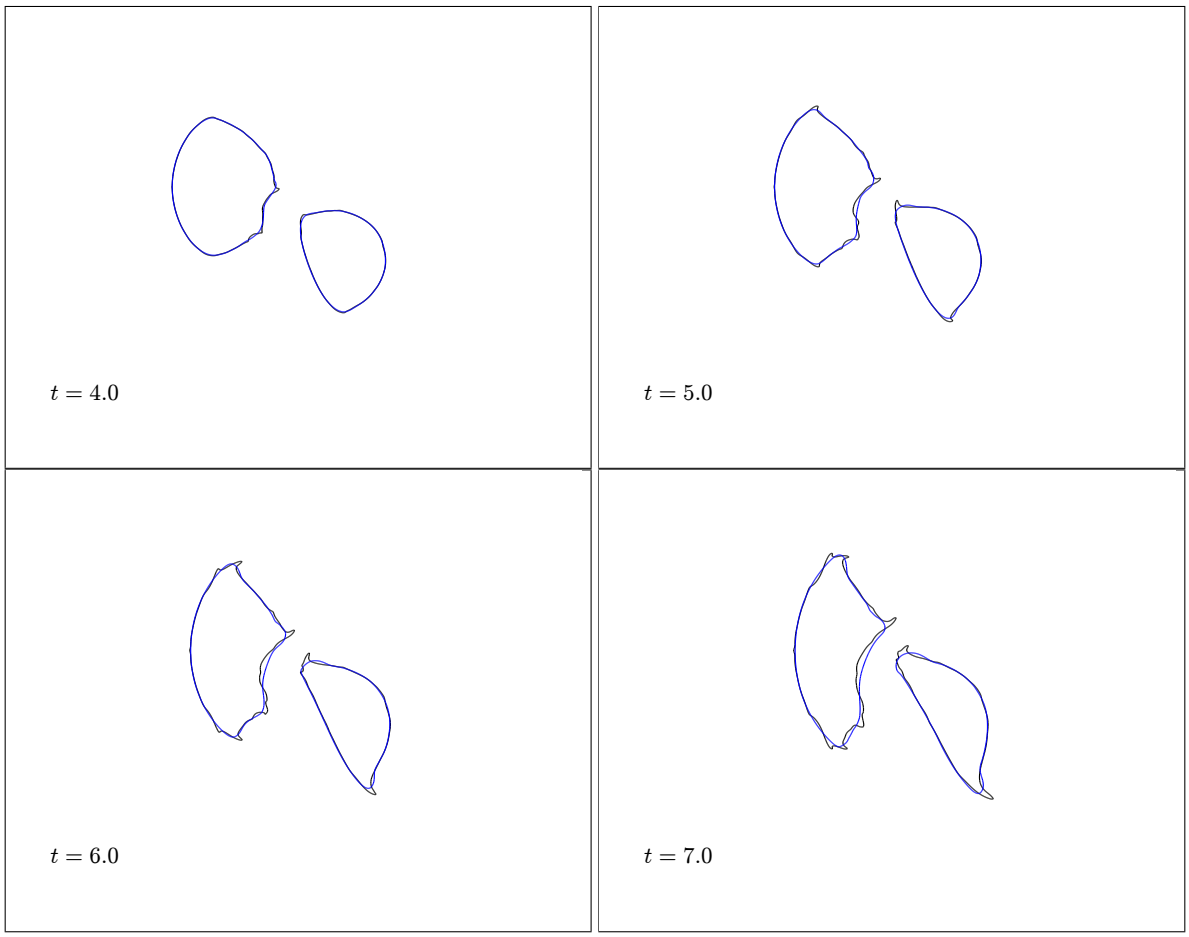

Figure 5. Dual water column shock interaction problem with surface tension. Solutions shown in non-dimensional time. Domain was discretized with a 1500×1250 grid. The lines show the location of the interface $\phi_l = 0.5$ for the case run with surface tension (blue) and without surface tension (black).

References

[1] Jinho Lee, Kuo-Cheng Lin, and Dean Eklund. *AIAA Journal*, 53(6):1405–1423, 2015.

[2] D. R. Guildenbecher, C. López-Rivera, and P. E. Sojka. *Experiments in Fluids*, 46(3):371–402, 2009.

[3] Mikhael Gorokhovski and Marcus Herrmann. *Annual Review of Fluid Mechanics*, 40:343–366, 2008.

[4] S. O. Unverdi and G. Tryggvason. *Journal of Computational Physics*, 100(1):25–37, 1992.

[5] G Tryggvason, B Bunner, A Esmaeeli, D Juric, N Al-Rawahi, W Tauber, J Han, S Nas, and Y J Jan. *Journal of Computational Physics*, 169:708–759, 2001.

[6] C.W Hirt and B.D Nichols. *Journal of Computational Physics*, 39(1):201–225, 1981.

[7] Rémi Abgrall and S Karni. *Journal of Computational Physics*, 169(2):594–623, 2001.

[8] Hiroshi Terashima and Grétar Tryggvason. *Journal of Computational Physics*, 228(11):4012–4037, 2009.

[9] Hiroshi Terashima and Grétar Tryggvason. *Computers and Fluids*, 39:1804–1814, 2010.

[10] Hong Luo, Joseph D. Baum, and Rainald Lohner. *Journal of Computational Physics*, 194(1):304–328, 2004.

[11] Keh-Ming Shyue. *Journal of Computational Physics*, 142:208–242, 1998.

[12] Richard Saurel and Rémi Abgrall. *SIAM Journal on Scientific Computing*, 21(3):1115–1145, 1999.

[13] Grégoire Allaire, Sébastien Clerc, and Samuel Kokh. *Journal of Computational Physics*, 181(2):577–616, 2002.

[14] Ratnesh K. Shukla. *Journal of Computational Physics*, 276:508–540, 2014.

[15] Eric Johnsen and Tim Colonius. *Journal of Computational Physics*, 219(2):715–732, 2006.

[16] Vedran Coralic and Tim Colonius. *Journal of Computational Physics*, 274:95–121, 2014.

[17] J. C. Meng and T. Colonius. *Shock Waves*, pp. 399–414, 2014.

[18] Ratnesh K. Shukla, Carlos Pantano, and Jonathan B. Freund. *Journal of Computational Physics*, 229(19):7411–7439, 2010.

[19] Denis Gueyffier, Jie Li, Ali Nadim, Ruben Scardovelli, and Stéphane Zaleski. *Journal of Computational Physics*, 152(2):423–456, 1999.

[20] Stephane Popinet and Stephane Zaleski. *International Journal for Numerical Methods in Fluids*, 30:775–793, 1999.

[21] Ruben Scardovelli and Stéphane Zaleski. *Annual Review of Fluid Mechanics*, 31:567–603, 1999.

[22] J. U. Brackbill, D.B. Kothe, and C. Zemach. *Journal of Computational Physics*, 100:335–354, 1992.

[23] Guillaume Perigaud and Richard Saurel. *Journal of Computational Physics*, 209(1):139–178, 2005.

[24] Moon S. Chung. *Applied Mathematical Modelling*, 31(3):578–588, 2007.

[25] Benjamin Braconnier and Boniface Nkonga. *Journal of Computational Physics*, 228(16):5722–5739, 2009.

[26] Nguyen T. Nguyen and Michael Dumbser. *Applied Mathematics and Computation*, 271:959–978, 2015.

[27] H. Chen. *AIAA Journal*, 46(5):1135–1143, 2008.

[28] D. J E Harvie, M. R. Davidson, and M. Rudman. *Applied Mathematical Modelling*, 30:1056–1066, 2006.

[29] Eleuterio F Toro. *Riemann Solvers and Numerical Methods for Fluid Dynamics: A Practical Introduction*. Springer, New York, 2009.

[30] Sigal Gottlieb and Chi-Wang Shu. *Mathematics of Computation*, 67(221):73–85, 1998.

[31] J P Cocchi, R Saurel, and J C Loraud. *Shock Waves*, 5(6):347–357, 1996.

[32] X.Y. Hu, N.A. Adams, and G. Iaccarino. *Journal of Computational Physics*, 228(17):6572–6589, 2009.

[33] Chih-Hao Chang and Meng-Sing Liou. *Journal of Computational Physics*, 225(1):840–873, 2007.

[34] Bruno Lafaurie, Carlo Nardone, Ruben Scardovelli, Stéphane Zaleski, and Gianluigi Zanetti. Modelling Merging and Fragmentation in Multiphase Flows with SURFER, 1994.

[35] Satoshi Ii, Sugiyama Kazuyasu, Shintaro Takeuchi, Shu Takagi, Yoichiro Matsumoto, and Feng Xiao. *Journal of Computational Physics*, 231:2328–2358, 2012.

[36] Elin Olsson, Gunilla Kreiss, and Sara Zahedi. *Journal of Computational Physics*, 225:785–807, 2007.

[37] Lord Rayleigh. *Proceedings of the Royal Society of London*, 29(196-199):71–97, 1879.

[38] D. E. Fyfe, E. S. Oran, and M. J Fritts. *Journal of Computational Physics*, 76:349–384, 1988.